THE ASTROPHYSICAL JOURNAL, 442:10–22, 1995 March 20

DUAL-FREQUENCY MAPPING WITH THE TENERIFE COSMIC MICROWAVE BACKGROUND EXPERIMENTS

C. M. GUTIÉRREZ DE LA CRUZ,[1,2] R. D. DAVIES,[2] R. REBOLO,[1] R. A. WATSON,[1,2]
S. HANCOCK,[3] AND A. N. LASENBY[3]

Received 1994 May 2; accepted 1994 September 28

ABSTRACT

We present maps of the sky at intermediate angular resolution (5°) of the declination range 35°.0–45°.0 obtained with the Tenerife cosmic microwave background (CMB) experiments using data up until 1992. The data were taken with beam-switching radiometers operating at 10.4 and 14.9 GHz. Right ascension scans were made at 2°.5 declination intervals centered on decl. +40° covering 3500 deg^2 of sky. The observations have been compared with known point sources and estimates of Galactic emission as a consistency check on the integrity of the data set. After subtraction of radio sources, the section of our data from R.A. 161° to 230° has been analyzed using a likelihood method with a Gaussian autocorrelation function. At 10.4 and 14.9 GHz we find evidence for fluctuations with intrinsic amplitudes of $\sqrt{C_0} = 41^{+26}_{-30}$ and 66^{+29}_{-22} μK (68% confidence limits), respectively, on a coherence scale of 4°. These levels are consistent with the expected rms sky signal from the *COBE* differential microwave radiometer first-year results and with the CMB signal detected at 14.9 and 33 GHz in the decl. = +40° strip by Hancock et al. (1994). Our results at 10.4 GHz set strong upper limits on the Galactic contamination at 14.9 GHz, suggesting that the signal found at the latter frequency is probably dominated by cosmological fluctuations.

Subject headings: cosmic microwave background — cosmology: observations — large-scale structure of universe

1. INTRODUCTION

Mapping of cosmic microwave background (CMB) structures provides a direct determination of the conditions prevailing in the universe during the epoch of recombination and, therefore, allows one to establish the basic parameters of cosmological models and theories of galaxy formation. Statistical detections of structure have been reported by the *COBE* (Smoot et al. 1992) and MIT (Ganga et al. 1993) groups, and several experiments are approaching sensitivities where the delineation of individual CMB features should be possible. Among these is the present Tenerife suite of experiments (Davies et al. 1987, 1992; Watson et al. 1992), which has now directly observed cosmological structure at decl. +40°.0 (Hancock et al. 1994).

We describe here the extension of the Tenerife CMB anisotropy experiments to a mapping mode, where a series of right ascension scans are made at half-beamwidth (2°.5) separation in declination. Such observations allow the delineation of structures with more confidence than with a single scan. Observations using scaled instruments with a common beam profile at 10.4 and 14.9 GHz give a first separation of the Galactic foreground emission from the intrinsic CMB and also allow limits to be set on the spectral index of the diffuse Galactic emission. Constraints on cosmological fluctuations will be established in terms of the two-point autocorrelation function using both a one-dimensional and a two-dimensional statistical analysis.

[1] Postal address: Instituto de Astrofísica de Canarias, 38200 La Laguna, Tenerife, Spain.
[2] University of Manchester, Nuffield Radio Astronomy Laboratories, Jodrell Bank, Macclesfield SK11 9DL, UK.
[3] Mullard Radio Astronomy Observatory, Cavendish Laboratory, Madingley Road, Cambridge CB3 0HE, UK.

2. METHOD OF OBSERVATION

The basic observing strategy and parameters are described in detail by Davies et al. (1992). Although they refer to the first experiment of the Tenerife series, the techniques are applicable to the subsequent experiments as well. In order to increase sensitivity to sky fluctuations, the beam size of the original 10.4 GHz radiometer (Davies et al. 1987) has been reduced from FWHM ~8° to ~5° by increasing the horn aperture while maintaining a beam switch of 8°.1. In addition, a scaled radiometer with the same angular resolution has been brought into operation at a frequency of 14.9 GHz. The switching circulator on the latter instrument is incorporated inside the cryostat in order to reduce system noise, and when combined with an increase of bandwidth from ~0.5 to ~1.0 GHz provides an improvement in sensitivity of a factor of 2 over the 10.4 GHz experiment.

The experiments use a drift scan technique in which the equipment is fixed relative to the ground, and scanning is achieved by using the Earth's rotation which sweeps the observing beams through the sky to give scans at fixed declination. The observing declination was selected by appropriately setting the elevation angle of the plane reflector which directed the sky signals into the horizontal microwave horns. To minimize any remaining effects due to the changing environment, such as the sky water-vapor content and the ambient temperature, a double subtraction technique was used combining fast switching (63 Hz) between the two horns and slower wagging (8 s) of the flat reflecting plate to switch the double beam by 8°.1 in right ascension. This produces the distinctive experiment profile of a positive beam on the meridian with two half-amplitude negative beams offset 8°.1 to the east and to the west. The beamwidths were calculated from horn models and observations to be 4°.9 ± 0°.2 and 5°.2 ± 0°.2 (FWHM) at 10.4 and 14.9 GHz, respectively.

The radiometers have a system of continuous on-line calibration produced by the injection of a modulated noise signal into the input waveguide, thereby providing an internal reference to remove gain drifts. The recorded data were converted to a brightness temperature scale by normalizing this internal calibrator source in terms of an absolute reference. An ambient temperature absorber, the Moon, and the Sun were all used as external calibrators. Two observing channels are employed at each frequency and when combined give theoretical sensitivities in the double-switched mode of 5.6 and 3.4 mK $Hz^{-1/2}$ at 10.4 and 14.9 GHz, respectively. Having two channels not only gives an improvement of a factor $\sqrt{2}$ in sensitivity but also permits a separation between combined atmospheric and sky signals, and instrumental effects.

Every 82 s the data acquisition program produces a block of data derived from the output of the radiometer channels and an external temperature-humidity probe. The strong Galactic plane crossing at R.A. $\sim 20^h$ is used to make a further daily check of the time alignment and the amplitude scale. The processed radiometer data consist of the total power level, the beam differences for each mirror position (first beam difference), the calibration signal, and the difference between the above beam differences (second beam difference), together with the calculation of the standard error in each quantity. Figure 1 shows these data streams at 14.9 GHz for a typical sidereal day (1991 September 17). Figures 1*a* and 1*b* show the unprocessed calibration signal and give the typical gain drifts that the system suffers due to the changing ambient temperature; the maximum drifts are $\sim 14\%$ and $\sim 5\%$ for channels 1 and 2, respectively. The system temperature plots in Figures 1*c* and 1*d* are made by dividing the total power counts by the calibration counts in order to remove the gain drifts caused by ambient temperature changes. It is clear that channel 2 system temperature still correlates with ambient temperature changes, and this effect is also seen in the first difference data (Figs. 1*e* and 1*f*). These long-term ($\gg 1$ hr) temperature effects are greatly reduced in the second beam difference data, since these are calculated directly as the difference between the two first beam differences where this effect is similar. The standard deviations of the second beam differences, as estimated from the scatter of the subintegrations within an 82 s cycle, are plotted in Figures 1*i* and 1*j*. The mean value of these estimates is seen to be 0.8 mK, except during a period in the late afternoon (R.A. = 220°–270° at this time of the year) which was affected by local water-vapor variations.

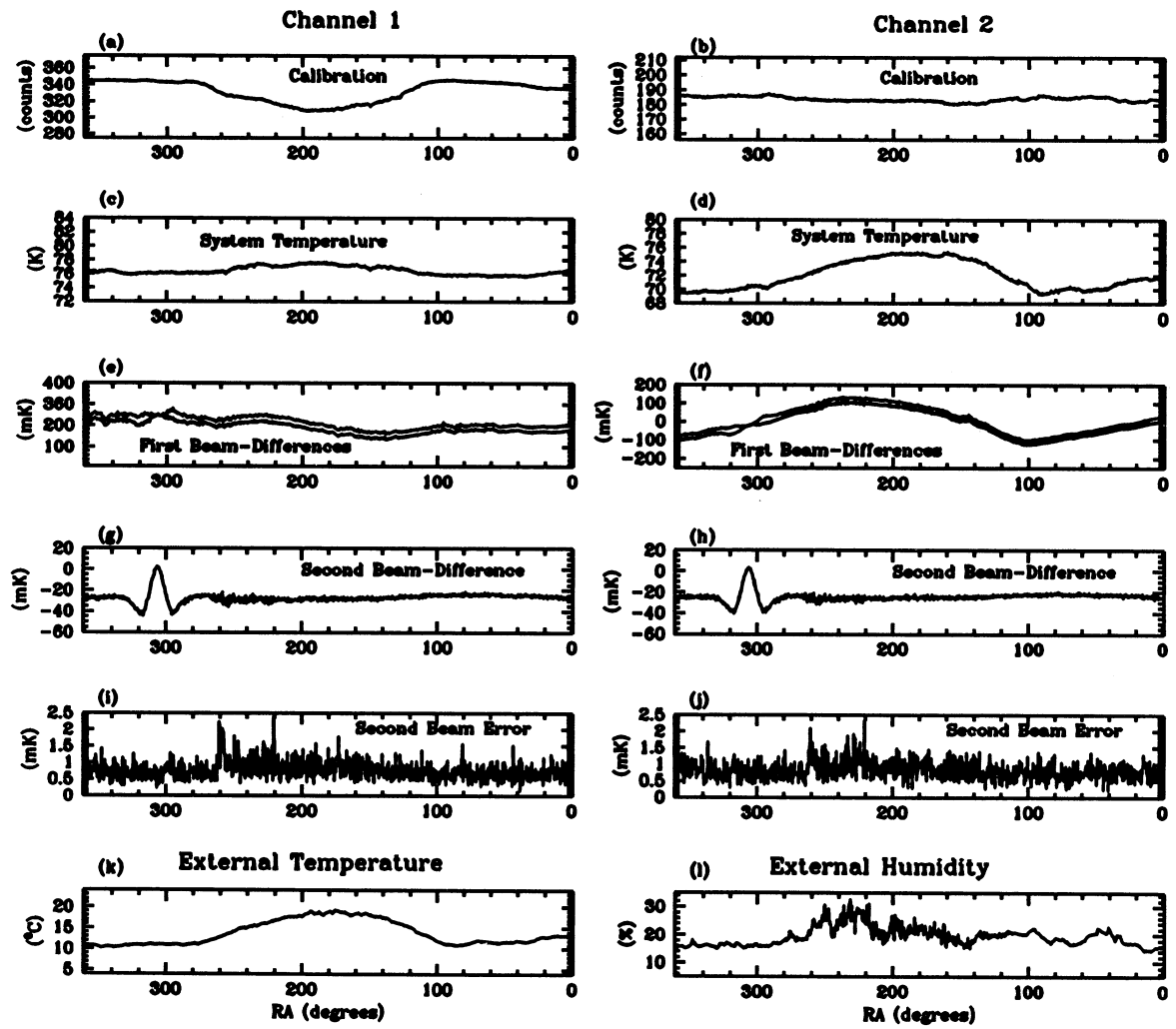

FIG. 1.—Data recorded on 1991 September 17 at 14.9 GHz. Plotted are the calibration signal (*a*, *b*), the total power (*c*, *d*), first differences in temperature (*e*, *f*), second differences (*g*, *h*), and the 1 σ error bars (*i*, *j*). The plots on the left and on the right are for channels 1 and 2, respectively. Panels (*k*) and (*l*) show, respectively, the external temperature and humidity for this day.

3. FIRST-STAGE ANALYSIS

We describe in this section the analysis of the data at 10.4 and 14.9 GHz up to the stage of producing a stacked scan for each declination observed. Our analysis is restricted to the 10.4 GHz measurements taken in the period 1986 June to 1991 September covering decl. 35°.0, 37°.5, 40°.0, 42°.5, and 45°.0, while the 14.9 GHz measurements were taken from 1990 May to 1992 April and covered decl. 37°.5, 40°.0, and 42°.5. The decl. = 40°.0 component of this data set represents ~70% of the 10.4 and 14.9 GHz data reported in Hancock et al. (1994) and at 14.9 GHz covers the same observing period as that described in Watson et al. (1992) with the quantity of 10.4 GHz data being increased by ~30%. The additional information contained within the scans at adjacent declinations offers improved definition of structures.

Approximately half of the time was taken up with maintenance, power cuts, and calibration runs. Further time was lost due to the weather, which affected the 14.9 GHz data more than 10.4 GHz data. Data were discarded when the Sun was closer than 50° to the main beam or the Moon was within 30°, and also when the observed standard error of an individual measurement was more than 3 times the value averaged over the day.

Before the beam-switched data from different observations at a given declination can be stacked, they are regridded into 4 minute bins in right ascension since the recording system is free-running in time. The residual long period baseline drifts after double differencing occur on timescales where the instrument is insensitive to astronomical signals (see Fig. 1) and are removed by a maximum entropy method (MEM) approach in which the common structure in each day of observation is solved for. This algorithm will be described in detail in a separate paper (Lasenby et al. 1995).

The final stacked scan was constructed from baseline-removed scans by the following method. The ith second difference mean temperature within the stacked scan ($\overline{\Delta T_i}$) was calculated by weighting over measurements for that position in the individual subscans, while the instrumental variance (σ_i^2) of the data was estimated from the corresponding distribution

$$\overline{\Delta T_i} = \frac{\sum_{j=1}^{n_i} \Delta T_{ij} w_{ij}}{\sum_{j=1}^{n_i} w_{ij}}, \quad (1)$$

$$\sigma_i^2 = \frac{\sum_{j=1}^{n_i} (\Delta T_{ij} - \overline{\Delta T_i})^2 w_{ij}}{\sum_{j=1}^{n_i} w_{ij}(n_i - 1)}, \quad (2)$$

where the indices ij refer to point i of scan j, ΔT_{ij} and w_{ij} are the second differences and weights within the subscans, and n_i is the number of scans included in the estimation. A weight was assigned to each point based on the scatter of the subintegrations within a 1° bin in right ascension.

Tables 1 and 2 show the mean number of measurements in a 1° bin in right ascension and the standard error over a beam-sized area, respectively. The noise does not strictly follow a $\sqrt{n}$ relation; this is a consequence of the change in sensitivity over the lifetime of the experiments due to technical improvements. The scans also do not have a uniform coverage as a consequence of seasonal effects, the most critical factors being bad weather in winter and the proximity of the Sun in the summer.

TABLE 1

MEAN NUMBER OF INDEPENDENT MEASUREMENTS PER 1° BIN OVER THE RANGE R.A. 1°–360°

Decl.	10.4 GHz	14.9 GHz
35°.0.....	26	...
37.5.....	21	10
40.0.....	84	102
42.5.....	24	27
45.0.....	24	...

TABLE 2

STANDARD ERROR (IN μK) PER BEAM-SIZED AREA OVER THE RANGE R.A. 1°–360°

Decl.	10.4 GHz	14.9 GHz
35°.0.....	129	...
37.5.....	147	97
40.0.....	106	50
42.5.....	142	63
45.0.....	149	...

These final stacked scans at each observed declination are shown in Figures 2 and 3 for 10.4 and 14.9 GHz. Figure 2 shows the prominent features at R.A. ~300° at each declination, which corresponds to the strong Galactic plane crossing, while the weak crossing is at R.A. = 60°–80°, as shown on an expanded scale in Figure 3. This weak crossing shows a double structure at lower declinations. Both crossings of the Galactic plane have lower amplitudes at 14.9 GHz as compared to 10.4 GHz as expected if free-free and synchrotron are the dominant processes.

The top sections of Figures 4 and 5 show the second difference temperature maps at 10.4 and 14.9 GHz, respectively, obtained by interpolating across the stacked scans in Figure 2 (note that an individual feature will have the characteristic triple-beam profile). A grid of 0°.5 × 0°.5 in right ascension and declination was used, followed by convolution with a Gaussian beam of FWHM = 4°. The bottom section of each figure shows the corresponding distribution of the noise. At both frequencies, the scan at decl. = +40°.0 has the lowest noise, as can be seen in Table 2. Both maps clearly show correlated structure produced by the crossings of the strong Galactic plane at R.A. ~ 300° and the weak one at R.A. ~ 60°–80°.

A feature can be seen at R.A. ~ 330° just after the strong Galactic crossing at 10.4 GHz with a corresponding weaker feature at 14.9 GHz, consistent with a source of Galactic origin, especially considering its proximity to the Galactic plane. In addition to this, there are two structures at 10.4 GHz centered at R.A. ~ 140° and ~250°, respectively; this last feature also appears in the 14.9 GHz map. In the next section we will show that the positions and amplitudes of both structures coincide with those expected for two known discrete radio sources. Furthermore, at R.A. ~ 225° we see a weak feature in the 10.4 GHz map, and its absence in the 14.9 GHz map indicates a possible Galactic origin. It is likely that this is the same feature reported in Davies et al. (1987) in the old (8° FWHM) version of the 10.4 GHz experiment. A numerical analysis of the features identified in the maps will be made in following sections.

4. SOURCES OF NONCOSMOLOGICAL SIGNAL

4.1. *Point Sources*

The contribution from known radio point sources can be estimated from the catalog by Kühr et al. (1981), which is complete down to 1 Jy at a frequency of 5 GHz. Additional infor-

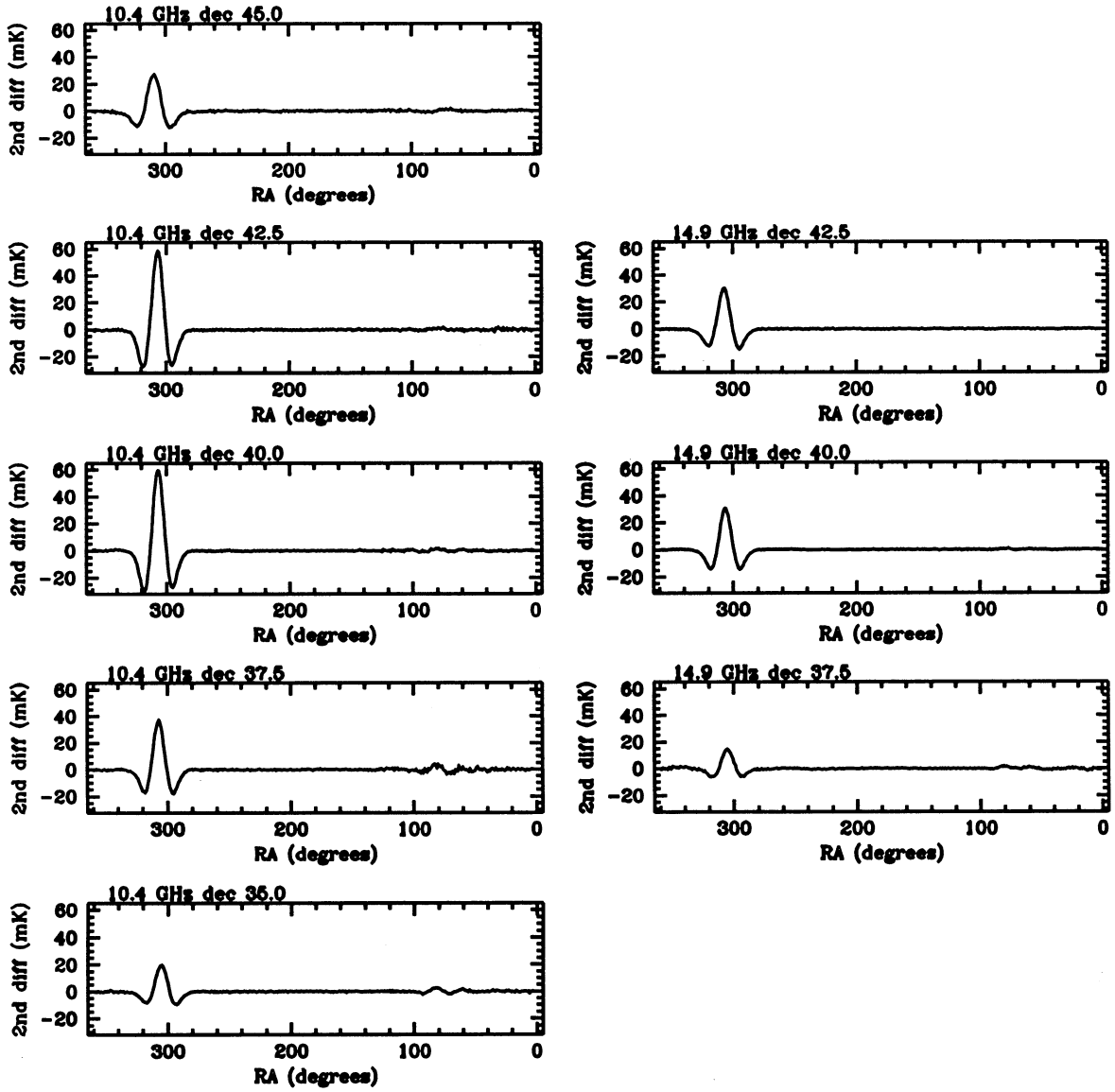

FIG. 2.—Stacked scans for each declination at 10.4 GHz (*left*) and 14.9 GHz (*right*) showing the strong (R.A. ~ 300°) and the weak (R.A. ~ 60°–80°) Galactic crossings. Data have been binned at 1° intervals in right ascension.

mation has been obtained from the Very Large Array calibrators list and from the Michigan bright radio source monitoring program operating during our observing epoch (M. Aller & H. Aller 1993, private communication). We convert fluxes to brightness temperature T_s (in kelvins) using

$$T_s = 10^{-26} \frac{\lambda^2}{2k} \frac{4 \ln 2}{\pi \mathrm{FWHM}^2} S ,$$

where the flux density S is given in janskys, the observing wavelength λ is in meters, the FWHM in radians, and k is the Boltzmann constant. In Figure 6 we have convolved the predicted temperatures for these radio sources with the triple beam of our instruments in order to estimate their contribution to our observations. The most intense of the sources in the Kühr catalog is 3C 84, R.A. = $3^h16^m29^s$, decl. = 41°19′ (J1950), which in our observations are mixed up with diffuse Galactic emission. The principal sources at high Galactic latitude are 0923+39 (4C 39.25) and 1641+39 (3C 345). The latter has an almost flat spectrum in the region 10–15 GHz, with its flux density at 10.4 GHz varying between 5 and 12 Jy during our observing epoch (M. Aller & H. Aller 1993, private communication). This is the dominant feature, away from the Galactic plane, centered at R.A. ~ 250° in the maps of Figures 4 and 5. Figure 7 shows a comparison between the modeled contribution of 3C 345 and the observational data taken at decl. = 40°.0; also included in this comparison is 1633+38, which is close to 3C 345 and makes a contribution ~15% to the modeled signal. At 10.4 GHz these radio sources constitute the dominant signal, and as expected, there is good agreement between the predicted and observed amplitude and morphology of the signal. In the 14.9 GHz data, their contribution is predicted to be a factor 2 lower, and again there is a reasonably good agreement of the observations with the predictions. The observed discrepancies at this higher frequency might be due to radio source variability over the duration of the observa-

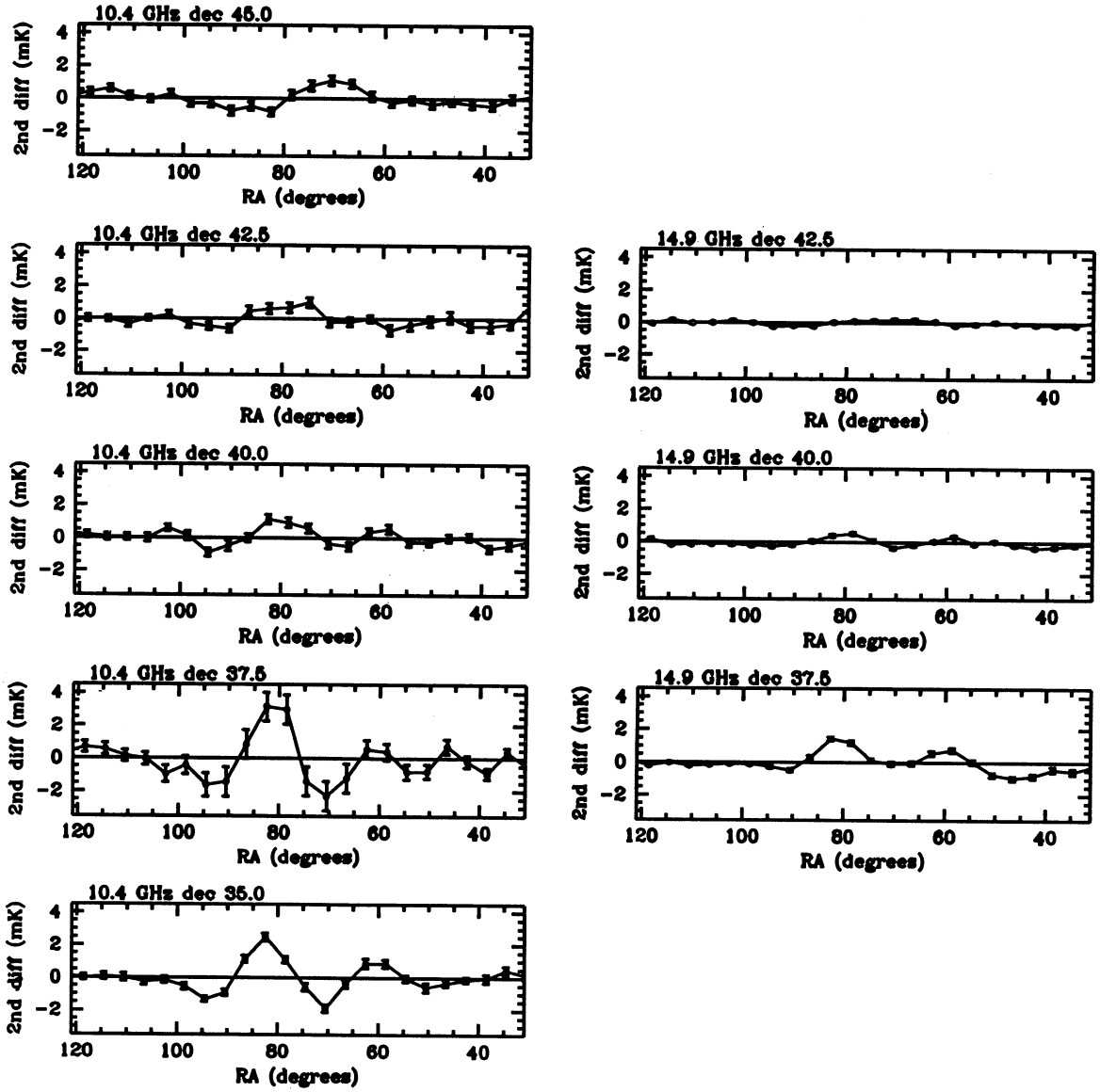

FIG. 3.—Expanded scale of Fig. 2 covering the region of the weak Galactic crossing and showing the 1 σ error bars. Data have been binned into 4° bins in right ascension.

tions or possibly as a direct result of the presence of CMB or Galactic emission which can make a relatively larger contribution to the reduced amplitude signal at 14.9 GHz. The observation of these radio sources with the predicted shape and amplitude confirms the consistency of our results. The point source 4C 39.25 at R.A. $\sim 140°$ is also clearly present in our data at 10.4 GHz (see map of Fig. 4), although its amplitude at 14.9 GHz (~ 100 μK) is below the 2 σ level in our data at this frequency.

The contribution due to the background of nonresolved sources at the frequencies of our experiments has been estimated by Franceshini et al. (1989). We have also made estimates of the contribution based on the source counts of Aizu et al. (1987) at 10 GHz. Both predictions agree that the temperature fluctuations $\Delta T/T$ induced by the background of randomly distributed sources should be less than 10^{-5} at 10.4 GHz. Making the conservative assumption of a flat spectrum for all the unresolved sources, they would contribute less than 5×10^{-6} at 14.9 GHz and are therefore below our present sensitivity.

4.2. *Galactic Emission*

To determine the possible contribution of Galactic emission we can use the available sky continuum maps below 1500 MHz. A detailed description of these is given in Lawson et al. (1987). We have considered the 408 MHz (Haslam et al. 1982) and the 1420 MHz maps (Reich & Reich 1988). The contribution of the CMB and the diffuse background of extragalactic radio sources were removed, after which point sources which contributed more than 0.1 and 0.01 K at 408 and 1420 MHz, respectively, were subtracted. The resulting maps should be dominated by Galactic free-free and synchrotron emission. We have converted these two maps to a common resolution and placed them on a common grid $1° \times 0°.5$ in right ascension and

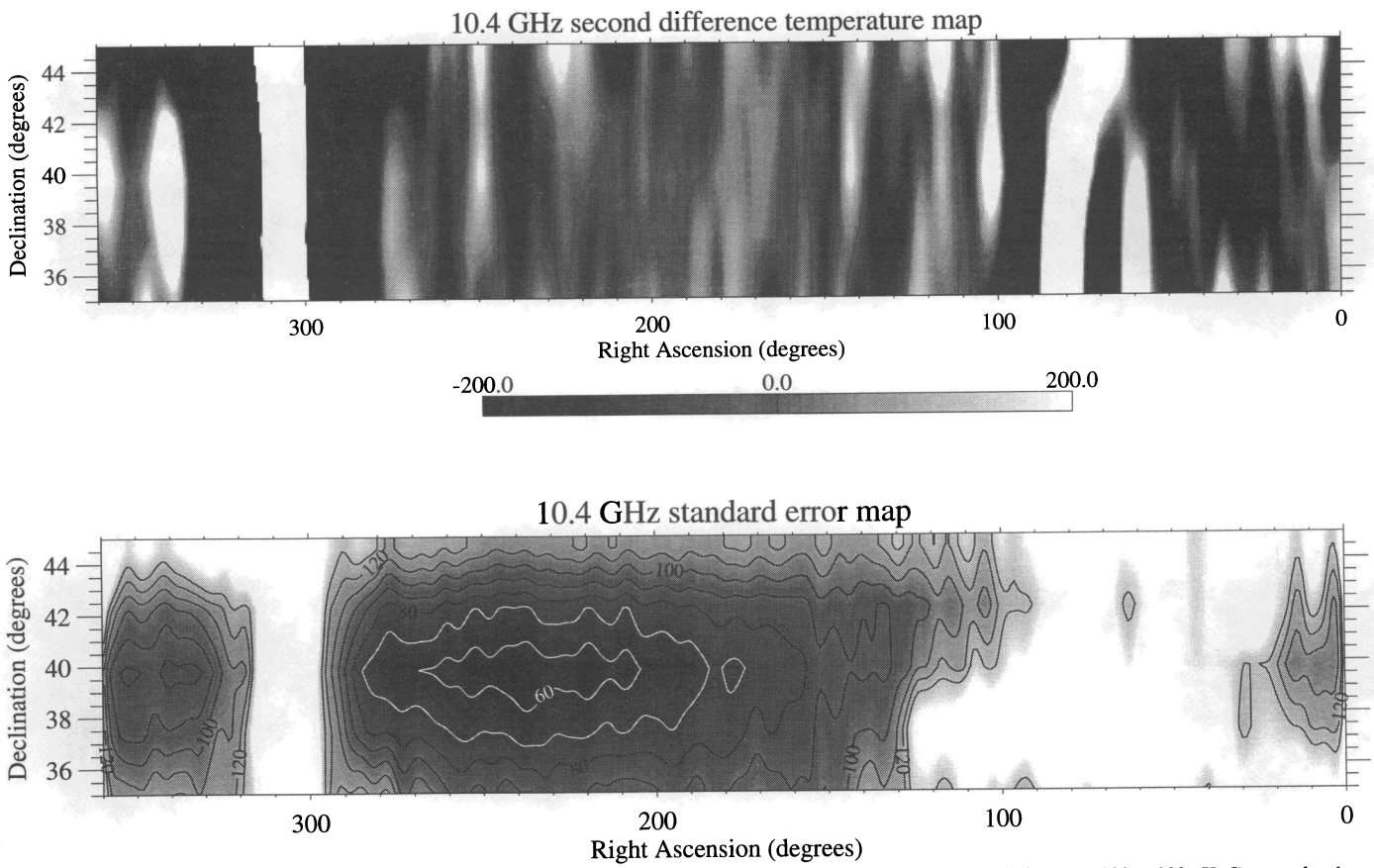

FIG. 4.—Second difference temperature map and the corresponding noise map (*bottom*) at 10.4 GHz. The gray-scale limits are −200 to 200 μK. Contour levels are every 20 μK in the temperature map and every 10 μK in the noise map.

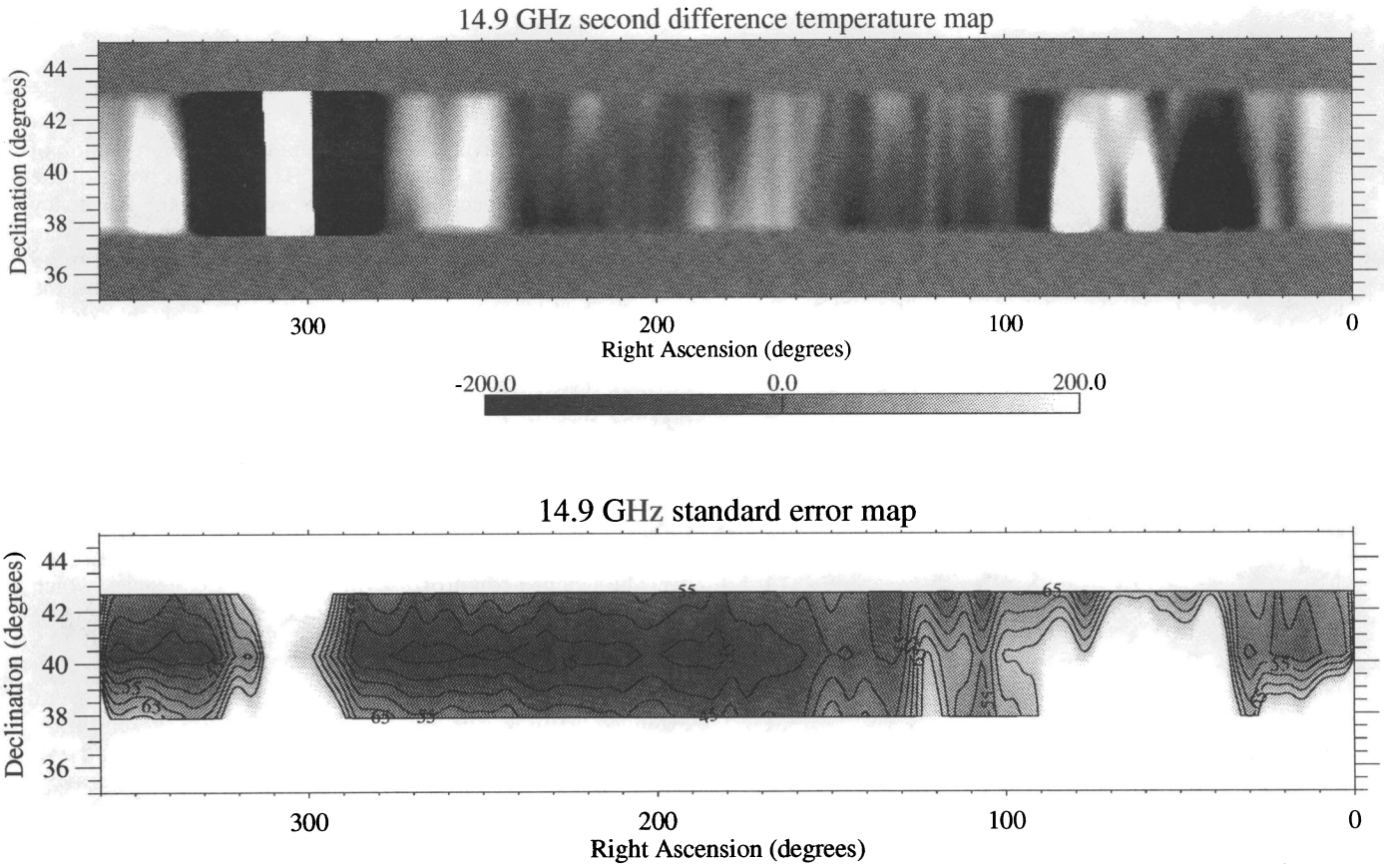

FIG. 5.—As for Fig. 4, but at 14.9 GHz with intervals of 5 μK in the noise map

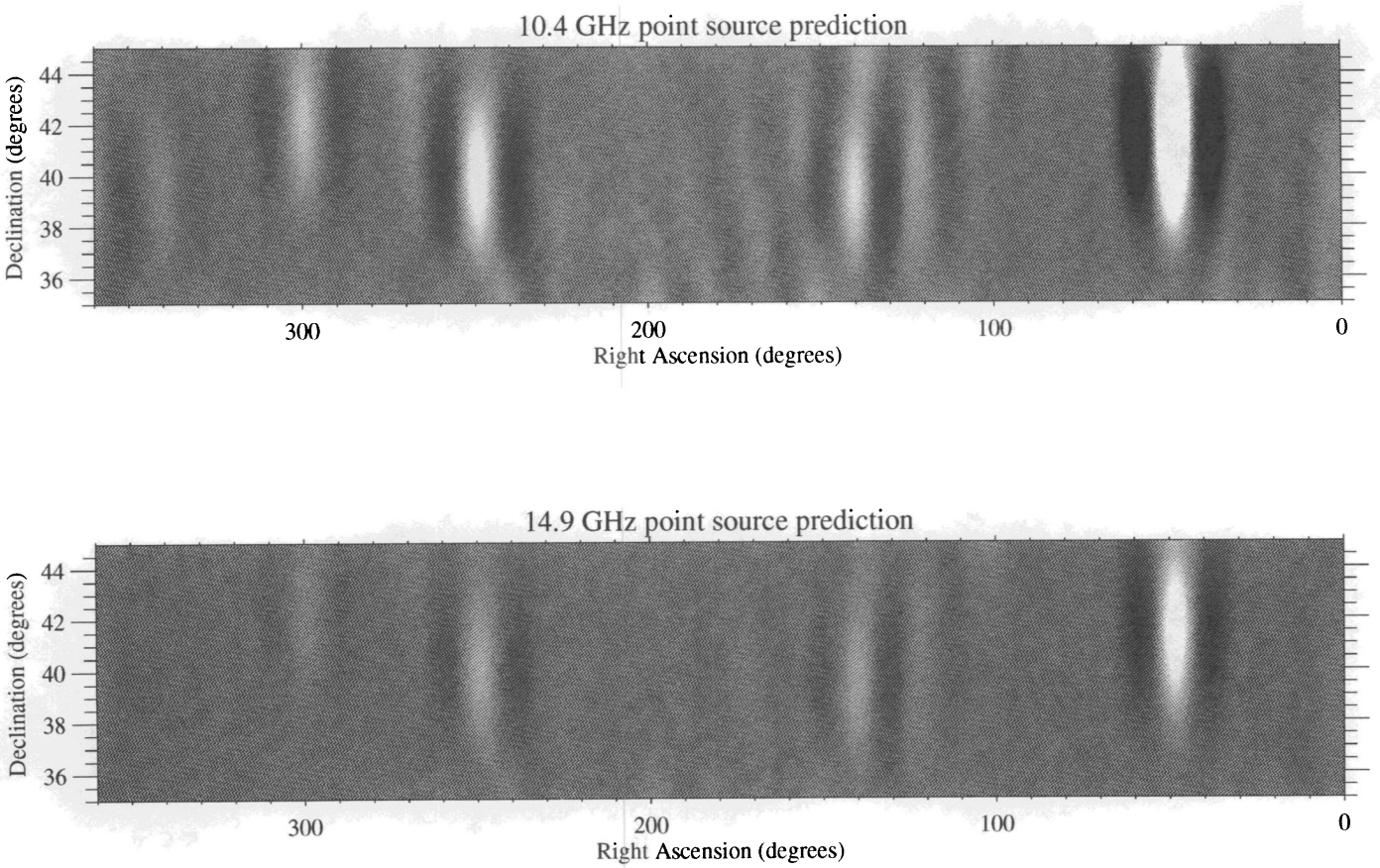

FIG. 6.—Map of estimated contribution of discrete radio sources at 10.4 GHz (*top*) and 14.9 GHz (*bottom*). The contour levels are every 20 μK.

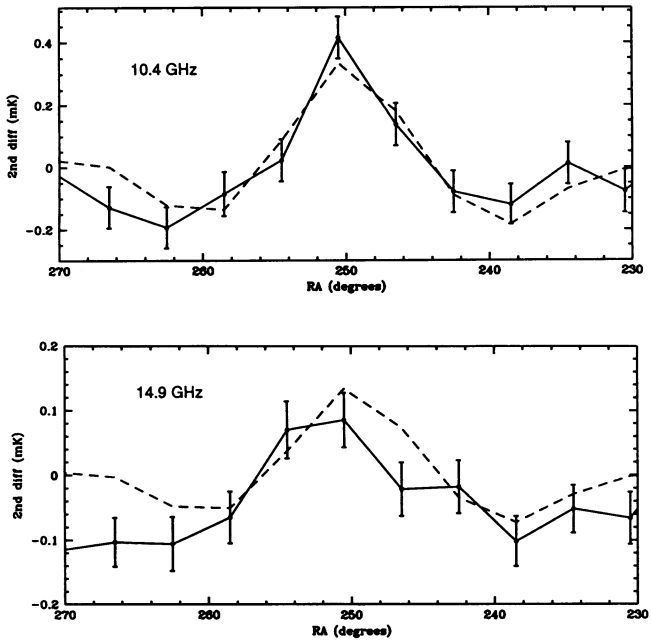

FIG. 7.—Comparison between the predicted contributions of the radio sources 3C 345 and 1633+38 at decl. = 40°, and our measurements with 1 σ error bars are indicated (*solid lines*).

declination, respectively. We used them to make a prediction of Galactic emission at 10.4 and 14.9 GHz for each point of the grid, assuming a spectral index independent of the frequency but varying spatially. These maps of predicted emission were convolved with our instrumental response. In Figures 8 and 9 we present the observations of the Galactic crossings and the corresponding predictions. In the direction of the strong Galactic crossing there exists a good spatial correlation both between the structures in the predicted and observed plots and between the structures seen at the different frequencies. We see that the measured signal is larger than the predicted one by a factor of 1.4–1.7 at 10.4 GHz and 1.5–2.2 at 14.9 GHz, depending on the declination considered. This indicates that the spectral index is flatter at our frequencies than at those of the survey maps and implies that our simple model is unrealistic. Our results are consistent with free-free emission dominating over the synchrotron processes at the higher frequencies, which is also reinforced by the spectral index deduced when comparing the amplitudes of the Galactic crossings at 10.4 and 14.9 GHz.

The weak Galactic plane at R.A. $\sim 60°$–$80°$ contains several extended features. The double-peaked structure present in the low-frequency survey is also clearly present at 10.4 and 14.9 GHz. The structure centered at R.A. $\sim 60°$ seems to have a flatter spectral index than the former, and it is not clearly present in the map at 408 MHz.

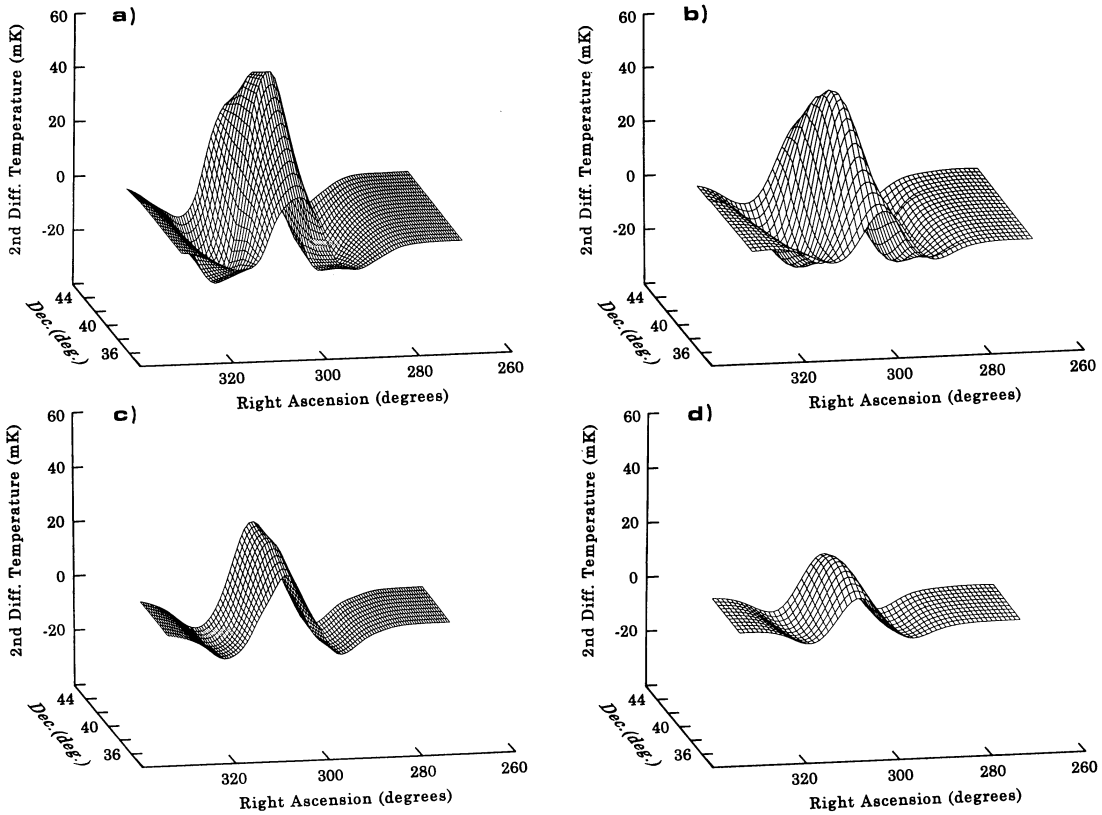

FIG. 8.—Comparison of the shape and amplitude of the observed major Galactic crossing (R.A. ~ 300°) at (*a*) 10.4 GHz and (*c*) 14.9 GHz with that predicted from low-frequency surveys at (*b*) 10.4 GHz and (*d*) 14.9 GHz; details of these predictions are given in the text. The 10.4 GHz data cover decl. 35°.0–45°.0, and the 14.9 GHz data cover decl. 37°.5–42°.5. The signal-to-noise ratio over the region shown is $\gtrsim 100$ for our observations.

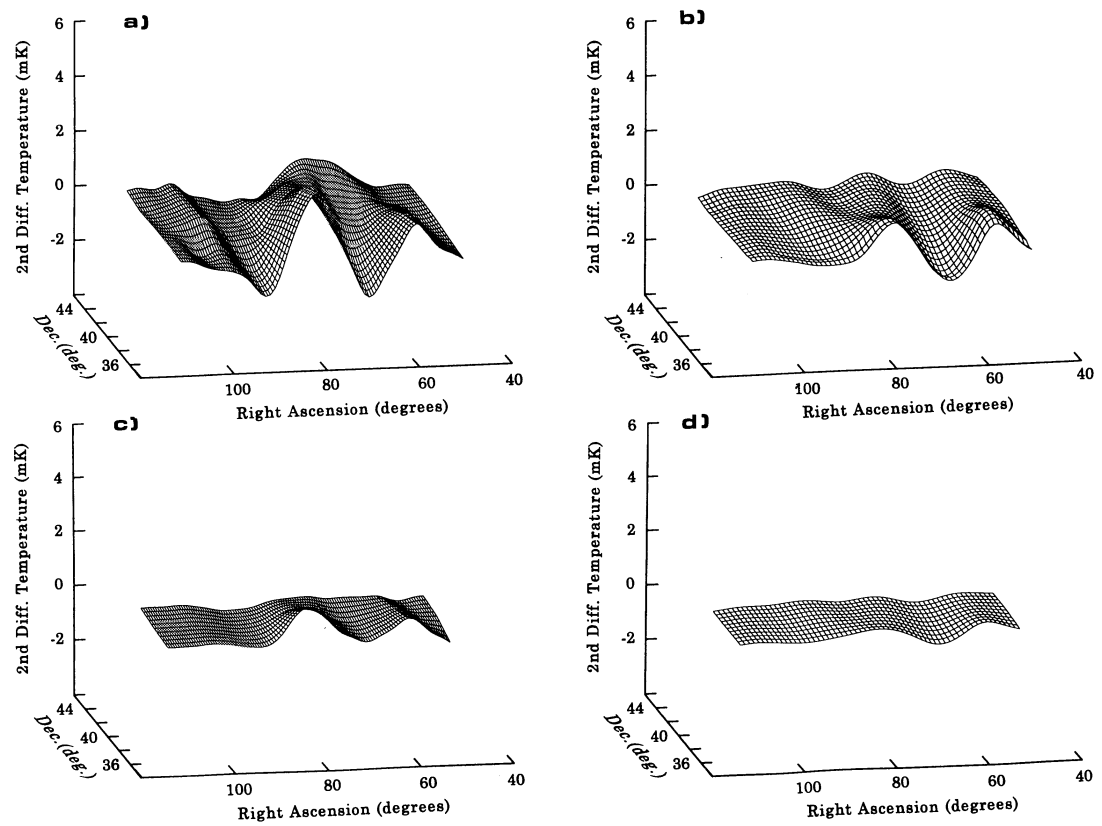

FIG. 9.—As for Fig. 8, but in the direction of the anticenter Galactic crossing (R.A. ~ 60°–80°): (*a*) 10.4 GHz and (*c*) 14.9 GHz observations, and (*b*) 10.4 GHz and (*d*) 14.9 GHz predictions. The signal-to-noise ratio varies between ~2 and ~5 for the observations shown.

We find the most intense signal at declinations 40°.0 and 42°.5 when the scan passes through the Cygnus region. At these frequencies the predominant contribution to the observed signal is due to H II emission from the extended Cygnus X H II complex (R.A. = 20^h26^m, decl. = 41°). In addition there is a contribution due to the presence of the extragalactic source Cygnus A (R.A. = 19^h58^m, decl. = 40°.6), but this is a factor of ~ 100 lower, and therefore it is possible to estimate the spectral index of the Galactic diffuse emission by comparing the signal in the low-frequency surveys with our measurements.

In Figure 10 we present a T-ν plot of the amplitudes of the strong Galactic crossings at each of the observed declinations using the surveys at 408 MHz and 1420 MHz and our measurements at 10.4 and 14.9 GHz. We consider a linear model with a constant spectral index between consecutive frequencies and take into account pointing errors in the declination due to uncertainties in mirror elevation which are estimated to be $\lesssim 0°.2$ on the sky. The spectral indices from 10.4 to 14.9 GHz are $2.6^{+0.6}_{-0.9}$, $1.9^{+0.3}_{-0.3}$, and $1.8^{+0.3}_{-0.3}$ at declinations 37°.5, 40°.0, and 42°.5, respectively. At declinations 40°.0 and 42°.5 (in the Cygnus X region) our results are consistent with free-free dominating over synchrotron emission at frequencies higher than 1420 MHz.

In general the predictions from low-frequency surveys ($\nu \leq 1.5$ GHz) in the high Galactic latitude region do not match the structures seen at our observing frequencies. One explanation for this inconsistency between the Galactic prediction and our data is that scanning effects and uncertainties in the base levels of the low-frequency maps at high Galactic latitudes make it impossible to use them to predict structure at high frequencies (Banday et al. 1991; Davies & Watson 1995). In the following sections we will consider in detail our data in the region R.A. $\sim$ 160°–230°, showing that it is possible to put strong constraints on cosmological fluctuations.

TABLE 3

MEAN NUMBER OF INDEPENDENT MEASUREMENTS PER 1° BIN OVER THE RANGE R.A. 161°–230°

Decl.	10.4 GHz	14.9 GHz
35°.0.....	31	...
47.5.....	21	10
40.0.....	101	85
42.5.....	27	25
45.0.....	20	...

5. STATISTICAL ANALYSES

Several methods have been developed to separate intrinsic CMB fluctuations from instrumental noise, and so in turn to set constraints on the amplitude of the CMB signal. Depending on the model considered and the experimental configuration, correlations may exist between adjacent data points. Therefore analysis techniques can make use of the different properties of noise and signal in order to characterize the data by its two-point autocorrelation function (ACF). The most common analyses are those using the likelihood function (Davies et al. 1987). This is used here as before in the single-declination analysis (Watson et al. 1992; Hancock et al. 1994) and is extended to a two-dimensional analysis by simultaneously considering data from two or more declinations.

We correct the data for the contribution of known discrete radio sources and restrict the analysis to the range $161° \leq$ R.A. $\leq 230°$ corresponding to Galactic latitude $b \geq 55°$. The data used are shown in Figure 11 binned at 1° intervals in right ascension and were obtained by weighted addition of the individual daily scans according to a weight derived from the average variance along the scan. Tables 3 and

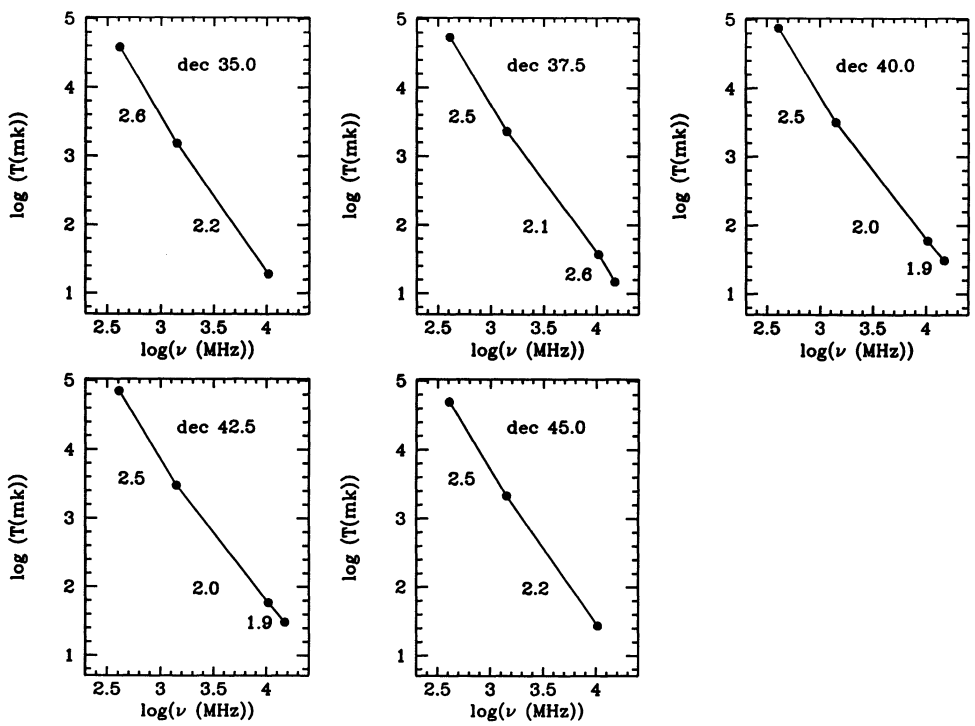

FIG. 10.—T-ν plots of the peak amplitude of the strong Galactic crossings in the surveys at 408 and 1420 MHz, and at our observing frequencies, showing the estimated spectral indices between consecutive frequencies.

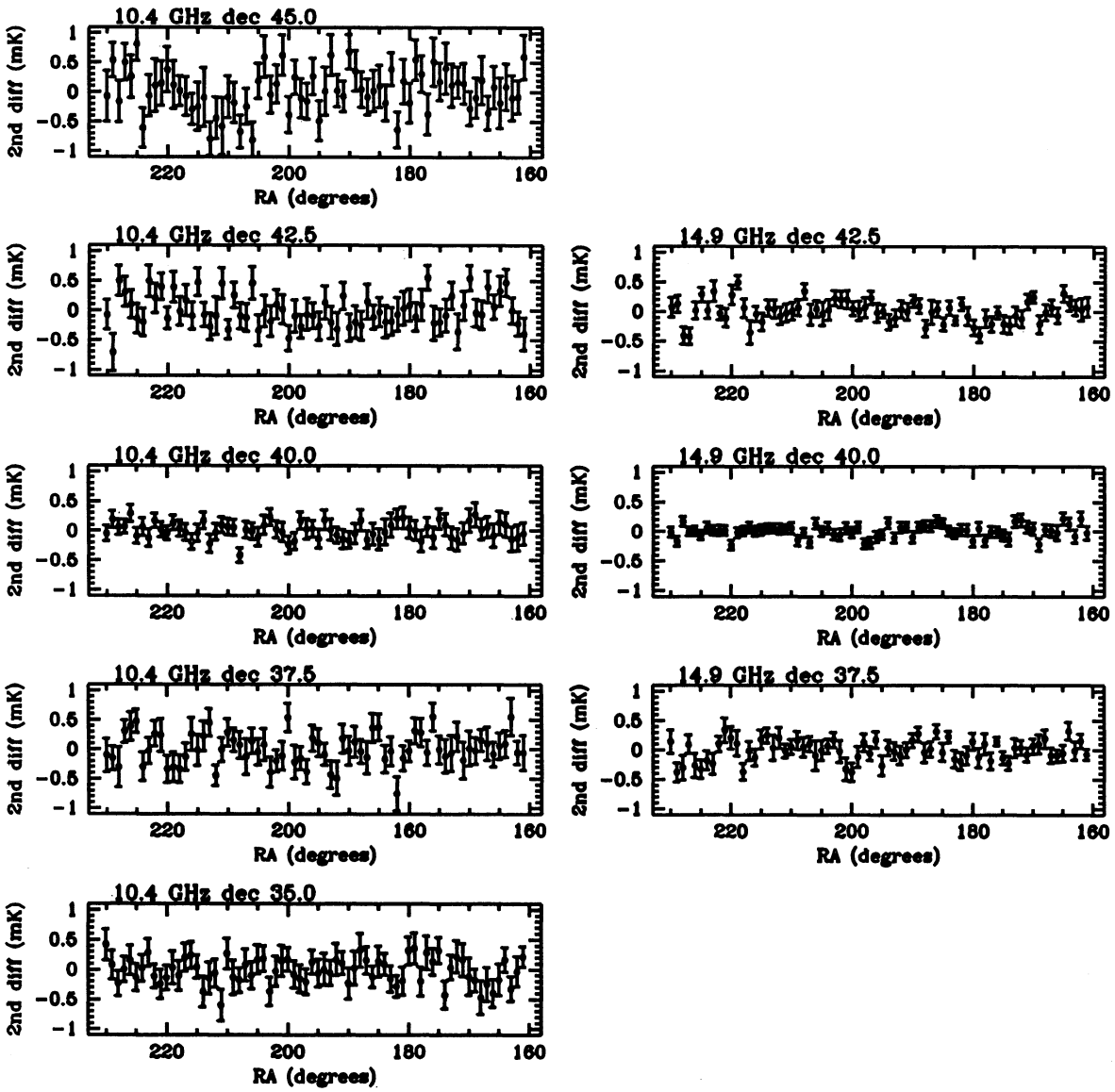

FIG. 11.—Difference in beam difference and the 1 σ error bars in the region at high Galactic latitude. The contributions of discrete radio sources have been removed. Data have been binned at 1° intervals in right ascension.

4 give the mean number of samples in a 1° R.A. bin and the standard error over a beam-sized area for the data shown in Figure 11.

We shall assume that CMB fluctuations are characterized by a two-dimensional, Gaussian random field and hence follow a multinormal distribution, in which their statistical properties are described entirely by their ACF, $C_{\rm intr}(0) = \langle \delta T(\hat{q}_1)\delta T(\hat{q}_2)\rangle$, where $\delta T(\hat{q})$ is the fluctuation in temperature in direction $\hat{q}$ and coordinates $\hat{q}_1$ and $\hat{q}_2$ are separated by an angle θ. Accordingly, for an experiment with the $-\frac{1}{2}+1-\frac{1}{2}$ switching pattern of the Tenerife instruments, the instrumental ACF measured between two points i and j with coordinates (α, δ) and (α', δ') is given by the covariance matrix

$$M_{ij} = \langle \{\delta T_m(\alpha, \delta) - \tfrac{1}{2}[\delta T_m(\alpha + \beta/\cos\delta, \delta) + \delta T_m(\alpha - \beta/\cos\delta, \delta)]\} \{\delta T_m(\alpha', \delta') - \tfrac{1}{2}[\delta T_m(\alpha' + \beta/\cos\delta', \delta') + \delta T_m(\alpha' - \beta/\cos\delta', \delta')]\}\rangle , \quad (3)$$

where $\delta T_m(\alpha, \delta)$ is the fluctuation in temperature at point (α, δ) after convolution with the Gaussian beam pattern for a single antenna and β is the switching angle. Taking into account the noise ϵ_i on observation i gives the total covariance matrix

TABLE 4

STANDARD ERROR (IN μK) PER BEAM-SIZED AREA OVER THE RANGE R.A. 161°–230°

Decl.	10.4 GHz	14.9 GHz
35°0.....	98	...
37.5.....	98	60
40.0.....	64	35
42.5.....	96	54
45.0.....	131	...

$V_{ij} = M_{ij} + \langle \epsilon_i \epsilon_j \rangle$, for which the last term is nonzero only for $i = j$ since the noise is uncorrelated from point to point.

Thus the likelihood function is given by

$$L(\Delta \boldsymbol{T} \mid y_1, y_2, \ldots, y_n) \propto \frac{1}{(\det \boldsymbol{V})^{1/2}} \exp\left(-\frac{1}{2} \Delta \boldsymbol{T}^T \boldsymbol{V}^{-1} \Delta \boldsymbol{T}\right), \tag{4}$$

where $y_1, y_2, \ldots, y_n$ are the model parameters and $\Delta \boldsymbol{T}$ is the data vector. For the sky model under consideration, one can then calculate the most probable model parameters in accordance with the data, by interpreting the resulting likelihood curves in a Bayesian sense, taking a uniform a priori probability distribution.

Following our previous analysis (Watson et al. 1992) we have considered a sky described by a Gaussian ACF which is characterized by the typical amplitude and angular scale of the fluctuations. Although not predicted in any particular cosmo logical scenario, this model is useful to compare results from different experiments. The functional form of the intrinsic ACF is then

$$C_{\rm intr}(\theta) = C_0 \exp\left(-\frac{\theta^2}{2\theta_c^2}\right), \tag{5}$$

where C_0 is the intrinsic variance of the sky and θ_c is the coherence angle. After filtering with an antenna with a Gaussian beam of dispersion σ, the ACF is expressed by

$$C_M(\theta, \sigma) \equiv \langle \delta T_m(\alpha, \delta)\, \delta T_m(\alpha', \delta') \rangle = \frac{C_0 \theta_c^2}{2\sigma^2 + \theta_c^2} \exp\left[\frac{-\theta^2}{2(2\sigma^2 + \theta_c^2)}\right]. \tag{6}$$

This is modified by the beam switching according to equation (3), from which one can identify the rms temperature fluctuation in a scan $\Delta T_{\rm rms}$, with the square root of the diagonal terms M_{ii}. It is found that the profile of this instrumental ACF is virtually independent of θ_c over the range 1°–10°, although the amplitude of $\Delta T_{\rm rms}/\sqrt{C_0}$, which defines the sensitivity to a given model, is a function of θ_c and attains a maximum at $\theta_c \sim 4°$ for the Tenerife experiments. In this case the relation between $\Delta T_{\rm rms}$ and $\sqrt{C_0}$ is $\Delta T_{\rm rms} \approx 0.75\sqrt{C_0}$.

The region analyzed covers $\sim$750 and $\sim$500 deg^2 at 10.4 GHz and 14.9 GHz, respectively, representing an increase in sky coverage by a factor of 2–3 over that presented in Hancock et al. (1994). It should be noted, however (see § 3), that the integration time at decl. = 40°.0 in the latter paper is larger than that presented here. In Tables 5 and 6 we give the resulting amplitudes, $\sqrt{C_0}$, of the intrinsic signal in the 10.4 and 14.9 GHz data for a model with coherence angle $\theta_c = 4°$. Column (1) of each table denotes the declinations incorporated in the analysis, while columns (2) and (3) give the signal amplitudes at 68% and 95% confidence, respectively. Considering first the results from the analysis of independent declinations separately, one finds marginal evidence for structure present in the 14.9 GHz decl. = 40°.0 and 37°.5 scans, at a level below the current sensitivity of the 10.4 GHz data and in accordance with the 10.4 GHz upper limits presented here. In our previous paper (Watson et al. 1992) using likelihood analysis of the decl. = +40° 14.9 GHz data presented there we placed a 95% confidence upper limit on structure at a level $\sqrt{C_0} = 51$ μK, although there were indications of features below this level in the MEM construction. The latter limit is compatible with the one presented here of 27^{+53}_{-27} μK and the detection limits of Hancock et al. (1994) which use an additional frequency at 33 GHz. At 10.4 GHz, in Watson et al. (1992), we found marginal evidence for structure at a level of 150 μK (from the peak of the likelihood curve). We did not set confidence limits to this result because we considered it too weak a detection. Due to the lack of error bounds we did not attempt a spectral fit to the 10.4 and 14.9 GHz data, instead consigning ourselves to a visual inspection of the MEM scans to tentatively suggest a most likely origin in Galactic emission. Our present analysis of the decl. = +40° 10.4 GHz data incorporates a more accurate calibration (including a reduction of 25% in the temperature scale) and a better baseline subtraction process (making simultaneous use of data from adjacent declinations) applied to an improved data set. This more rigorous analysis allows us to set an upper limit of 85 μK at 95% confidence and demonstrates that the spectrum is inconsistent with that from Galactic emission and is in agreement with a blackbody. At decl. = 42°.5 structure is detected at an amplitude of order 100 μK at both frequencies and could be explained to be the result of a combination of CMB and Galactic emission. The situation at decl. = 45°.0 is somewhat confusing, with a relatively large amplitude signal present at the 2.5 σ level. Without further spectral information the origin of this signal is uncertain, although its relatively high amplitude is more consistent with a Galactic origin, given that the typical amplitude of CMB structures on these scales is expected to be $\sim$50 μK (see Hancock et al. 1994; and § 6). The stability of the signals at decl. 42°.5 and 45°.0 has been investigated by the analysis of independent splits of the data set, but the results are inconclusive due to the reduced sensitivity resulting from the limited amount of data; future observations should clarify this situation. The joint analysis of the combined common coverage of decl. 37°.5, 40°.0, and 42°.5 at the two observing frequencies provides greater sensitivity, to structures in the data. The likelihood curves for this combined data set are depicted in Figure 12 and show evidence of structure at a similar level ($\sqrt{C_0} = 41$–66 μK) at both frequencies. These results, as shown in the first row of Tables 5 and 6, are in agreement with the analysis of each declination separately and offer improved evidence for the presence of structure at an amplitude $\sqrt{C_0} \sim 50$ μK. The analysis of different sets of declinations also gives detections compatible with the previous result, confirming the evidence for structures present at comparable amplitudes in the different scans.

TABLE 5

RESULTS OF THE LIKELIHOOD ANALYSIS FOR DATA OVER THE RANGE R.A. 161°–230° AT 10.4 GHz

Decl. (1)	$\sqrt{C_0}$ (μK) 68% CL (2)	$\sqrt{C_0}$ (μK) 95% CL (3)
37°.5–40°.0–42°.5	41^{+26}_{-30}	41^{+60}_{-41}
37°.5–40°.0	≤40	≤81
40°.0–42°.5	33^{+26}_{-33}	33^{+77}_{-33}
45°.0	178^{+97}_{-68}	178^{+230}_{-123}
42°.5	85^{+55}_{-70}	85^{+145}_{-85}
40°.0	≤40	≤85
37°.5	≤65	≤143
35°.0	≤63	≤145

TABLE 6

RESULTS OF THE LIKELIHOOD ANALYSIS FOR DATA OVER THE RANGE R.A. 161°–230° AT 14.9 GHz

Decl. (1)	$\sqrt{C_0}$ (K) 68% CL (2)	$\sqrt{C_0}$ (K) 95% CL (3)
37°.5–40°.0–42°.5.....	66^{+29}_{-22}	66^{+66}_{-39}
37°.5–40°.0	39^{+22}_{-15}	39^{+51}_{-30}
40°.0–42°.5	56^{+35}_{-24}	56^{+90}_{-43}
42°.5	120^{+57}_{-40}	120^{+139}_{-70}
40°.0	27^{+20}_{-21}	27^{+53}_{-27}
37°.5	57^{+39}_{-31}	57^{+83}_{-57}

6. DISCUSSION OF RESULTS

By considering that the statistical detection reported by Smoot et al. (1992) is produced by cosmological fluctuations, we can compute what signal would be expected in the Tenerife experiments and compare it with our results. From the reported rms signal 30 ± 5 μK in a 10° beam, the corresponding intrinsic signal for the model considered here can be calculated using equation (6), giving $\sqrt{C_0} = 54 \pm 9$ μK, which is fully compatible with our findings.

We will now consider whether the signal detected in our 14.9 GHz data is mostly due Galactic contamination or to cosmological fluctuations. To differentiate between them we have to estimate the likely contribution of the Galaxy. As we have seen (§ 4), the low-frequency surveys are unsuitable for a prediction of the Galactic emission in the 10–15 GHz range; however, recalling that the 10.4 and 14.9 GHz experiments have the same beam geometry, we can use our 10.4 GHz data to set an upper limit to the diffuse Galactic emission present in the 14.9 GHz observations. Under the conservative assumption that the maximum signal compatible with the 10.4 GHz data ($\Delta T_{\rm rms} \approx 0.75\sqrt{C_0} \leq 80$ μK at 95% confidence level) is Galactic in origin with a spectral index of 2.1 corresponding to free-free emission, we obtain a maximum value of $\Delta T_{\rm rms} \leq 38$ μK for the Galactic contribution at 14.9 GHz in the region 37°.5–42°.5. If we assumed synchrotron emission with a spectral index of 2.8, the signal would be $\Delta T_{\rm rms} \leq 29$ μK at the 95% confidence level. Both results are below the most probable signal in our data at 14.9 GHz ($\Delta T_{\rm rms} \approx 0.75\sqrt{C_0} = 50$ μK) and, given the signal level expected from the *COBE* detection, indicate the fluctuations of cosmological origin could indeed be the most significant contributor at this frequency.

Mapping with our new radiometer at 33 GHz should definitely solve the question of the cosmological origin for the structure at 14.9 GHz. Even assuming the less favorable case that free-free rather than synchrotron emission is the dominant process at 10.4 GHz and taking the 95% upper limit of the signal, its contribution at 33 GHz should be $\Delta T_{\rm rms} \leq 7$ μK and most probably only 3 μK, at least a factor 10 below the expected level of cosmological fluctuations. Our first results including data at this frequency have already demonstrated (Hancock et al. 1994) the existence of cosmological structure at a level $\Delta T_{\rm rms} = 42$ μK in the decl. = 40°.0 scan and thus support the possibility of a sizeable CMB component to the signals at adjacent declinations.

7. CONCLUSIONS

We have presented observations made with the Tenerife beam-switching radiometers at 10.4 and 14.9 GHz in the region covering decl. 35°.0–45°.0, and 37°.5–42°.5, respectively. The best quality data have been obtained with the 14.9 GHz radiometer at decl. = 40°.0, where the sensitivity is better by a

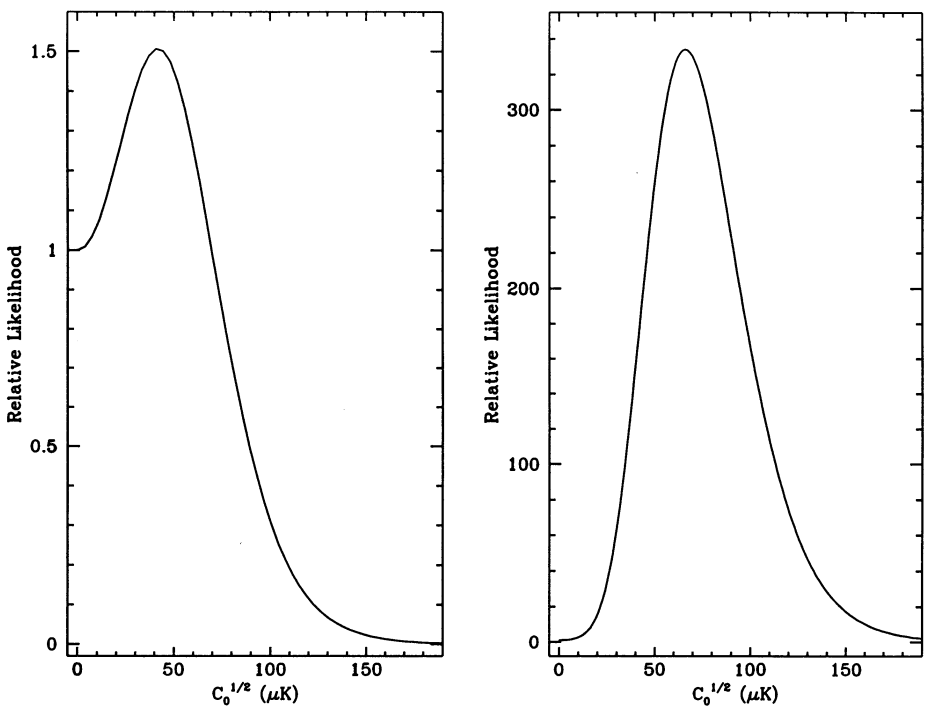

FIG. 12.—Likelihood curves for 10.4 GHz (*left*) and 14.9 GHz (*right*) assuming a sky model described by a Gaussian ACF function with a coherence angle of 4°. The region of the sky analyzed contains data at decl. = 37°.5, 40°.0, and 42°.5 from R.A. 161°–230°.

factor of 1.5–2 than at adjacent declinations. Maps at 10.4 and 14.9 GHz have been produced and attain peak sensitivities of 64 and 35 μK per beam area at the respective frequencies. Our data show a clear internal correlation between structures in the region of the Galactic plane and also correlate with the predictions from low-frequency Galactic-dominated surveys. Our results show that the spectral index of the emission in the Galactic plane is lower at higher frequencies and that free-free emission dominates over synchrotron emission at frequencies larger than 1420 MHz. The radio source 3C 345, the brightest in the high Galactic latitude region of our map, is detected with the expected shape and amplitude, ($\sim$300 and $\sim$100 μK at 10.4 and 14.9 GHz, respectively), giving further confidence to our measurements.

After subtraction of point sources, the high Galactic latitude data in the range $161° \leq$ R.A. $\leq 230°$ were analyzed statistically to constrain the amplitude of fluctuations. The results of this analysis show evidence of the presence of signal with an intrinsic amplitude of $\sqrt{C_0} = 41^{+26}_{-30}$ μK at 10.4 GHz and $\sqrt{C_0} = 66^{+29}_{-22}$ μK (68% confidence limits) at 14.9 GHz for Gaussian ACF models with a coherence angle $\theta_c = 4°$. Using our 10.4 GHz data to place limits on the Galactic contamination at 14.9 GHz we conclude that cosmological fluctuations could be the most significant contributor to the signal at this frequency. These results are compatible with the statistical detection by the *COBE* group, and also with our previous detection of CMB features in the decl. = 40°.0 strip (Hancock et al. 1994). The results presented here extend the latter detection of structure at 10.4 and 14.9 GHz to a larger sky area, and future mapping at 33 GHz, now in progress, will distinguish between a Galactic and a cosmological origin for the structures in this extended region.

Our thanks go to all of the staff at NRAL and the IAC who have contributed to these results. This work has been partly supported by the SERC, the DGICYT, and EU Science SC1-CT92-830 grant. S. H. wishes to acknowledge a Research Fellowship at St. John's College, Cambridge, UK.

REFERENCES

Aizu, K., Inoue, M., Tabara, H., & Kato, T. 1987, in IAU Symp. 124, Observational Cosmology, ed. A. Hewitt, G. Burbidge, & C. Z. Fang (Dordrecht: Reidel), 565
Banday, A. J., Giler, M., Szabelska, B., Szabelski, J., & Wolfendale, A. W. 1991, ApJ, 375, 432
Davies, R. D., Lasenby, A. N., Watson, R. A., Daintree, E. J., Hopkins, J., Beckman, J., Sanchez-Almeida, J., & Rebolo, R. 1987, Nature, 326, 462
Davies, R. D., & Watson, R. A. 1995, in preparation
Davies, R. D., Watson, R. A., Daintree, E. J., Hopkins, J., Lasenby, A. N., Sanchez-Almeida, J., Beckman, J. E., & Rebolo, R. 1992, MNRAS, 258, 605
Franceschini, A., Toffolatti, L., Danese, L., & De Zotti, G. 1989, ApJ, 344, 35
Ganga, K., Cheng, E., Meyer, S., & Page, L. 1993, ApJ, 410, L57
Hancock, S., Davies, R. D., Lasenby, A. N., Gutierrez de la Cruz, C. M., Watson, R. A., Rebolo, R., & Beckman, J. E. 1994, Nature, 367, 333
Haslam, C. G. T., Salter, C. J., Stoffel, H., & Wilson, W. E. 1982, A&AS, 47, 1
Kühr, H., Witzel, A., Pauliny-Toth, I. I. K., & Nauber, U. 1981, A&AS, 45, 367
Lasenby, A. N., et al. 1995, in preparation
Lawson, K. D., Mayer, C. J., Osborne, J. L., & Parkinson, M. L. 1987, MNRAS, 225, 307
Reich, P., & Reich, W. 1988, A&AS, 74, 7
Smoot, G. F., et al. 1992, ApJ, 396, L1
Watson, R. A., Gutierrez de la Cruz, C. M., Davies, R. D., Lasenby, A. N., Rebolo, R., Beckman, J. E., & Hancock, S. 1992, Nature, 357, 660